On Macrosegregation

ANDREAS LUDWIG, MENGHUAI WU, and ABDELLAH KHARICHA

Macrosegregations, namely compositional inhomogeneities at a scale much larger than the microstructure, are typically classified according to their metallurgical appearance. In ingot castings, they are known as 'A' and 'V' segregation, negative cone segregation, and positive secondary pipe segregation. There exists 'inverse' segregation at casting surfaces and 'centerline' segregation in continuously cast slabs and blooms. Macrosegregation forms if a relative motion between the solute-enriched or -depleted melt and dendritic solid structures occurs. It is known that there are four basic mechanisms for the occurrence of macrosegregation. In the recent years, the numerical description of the combination of these mechanisms has become possible and so a tool has emerged which can be effectively used to get a deeper understanding into the process details which are responsible for the formation of the above-mentioned different macrosegregation appearances. Based on the most sophisticated numerical models, we consequently associate the four basic formation mechanisms with the physical phenomena happening during (i) DC-casting of copper-based alloys, (ii) DC-casting of aluminum-based alloys, (iii) continuous casting of steel, and (iv) ingot casting of steel.

DOI: 10.1007/s11661-015-2959-4

I. INTRODUCTION

DURING solidification of alloys, the solid usually has a lower composition compared to the liquid from which it crystallizes. The corresponding solute redistribution leads to an accumulation of solute in the melt at the solid/liquid interface and thus to a constantly changing composition of the solid layers that form. The solute enrichment of the remaining liquid continues until the occurrence of a low melting point phase finally completes the solidification process. The resulting inhomogeneity of the solute elements is termed as microsegregation as it occurs on the scale of the growing crystals, the scale of the microstructure that forms.[1]

On the other hand, the solute composition may also vary on the scale of the whole casting. Such macroscopic inhomogeneities of solute elements are termed as macrosegregation.[2] The difference between microsegregation and macrosegregation is that macrosegregation cannot be removed by heat treatment as diffusion in solids is slow even for elevated temperatures and large diffusion distances might result in impracticably long holding times for homogenization.

A review of the history of publications on macrosegregation (started as early as 1540 A.D.) can be found in Reference 3. From the pioneering work of Kirkaldy mentioned in Reference 4 and Flemings *et al.* in the latter half of the 1960s,[5–7] it is well known that macrosegregation may form when the (micro)segregated melt adjacent to some solid is swept away by a relative motion between the solid and its surrounding liquid. The following six major phenomena have been identified as the reasons for such a relative motion[8]:

- forced flows due to pouring, gas purging, mechanical and electromagnetic stirring, *etc.*;
- buoyancy-induced flows due to thermal and solutal gradients in the liquid;
- flow that feeds the solidification shrinkage and the contractions of the liquid and solid during cooling;
- movement of free (equiaxed) grains or solid fragments;
- deformation of the solid network due to thermal stresses, metallostatic head, or external forces on the solid shell;
- motion of gas bubbles that develop during solidification.

As melt flows, it is not easy to quantify the motion of crystals and deformation of a solid skeleton, and thus reports on macrosegregation formation often limit themselves to one of the following four cases: (i) DC-casting of copper-based alloys, (ii) DC-casting of aluminum-based alloys, (iii) continuous casting of steel, and (iv) ingot casting of steel. In the present paper, general considerations on macrosegregation formation are applied to all four of these industrially relevant cases in order to elucidate mechanisms which they have in common. Hereby, we focus on a qualitative analysis of the corresponding formation of macrosegregation, as numerous quantitative analyses are reported in the literature and will be cited when the different cases are discussed.

ANDREAS LUDWIG, Full Professor, is with the Chair of Simulation and Modeling of Metallurgical Processes, Montanuniversitaet Leoben, Leoben, Austria. Contact e-mail: ludwig@unileoben.ac.at MENGHUAI WU, Associate Professor, and ABDELLAH KHARICHA, Senior Scientist, are with the Chair of Simulation and Modeling of Metallurgical Processes, Montanuniversitaet Leoben, and also with the Christian-Doppler Laboratory for Advanced Process Simulation of Solidification and Melting, Montanuniversitaet Leoben.
Manuscript submitted September 20, 2014.
Article published online May 19, 2015

II. MECHANISMS OF MACROSEGREGATION FORMATION

A. *Basic Mechanisms*

Local solidification processes have been successfully analyzed using the so-called "Representative Volume Element" (RVE). An RVE is considered as the volume at a certain position in space that is large enough to include multiple microstructure features and small enough that the important variations in the temperature, enthalpy, and volume fraction of the different phases are resolved.[2] This RVE is generally considered as a closed volume so that no mass or species is allowed to enter or leave the volume. By considering a given cooling behavior of such an RVE, the formation of microsegregation was analyzed and successful models such as the Gulliver–Scheil,[9,10] or Brody–Flemings,[11] or Clyne–Kurz[12] were derived.

However, for the analyses of the formation of macrosegregation, the RVE must be considered to be opened so that mass and/or species may enter or leave the RVE. As is commonly done, in this paper, macrosegregation is measured by means of the mixture concentration, C_{mix}, as

$$C_{\text{mix}} := \frac{g_l \rho_l \bar{C}_l + g_c \rho_c \bar{C}_c + g_e \rho_e \bar{C}_e}{g_l \rho_l + g_c \rho_c + g_e \rho_e} \qquad [1]$$

with g_l, g_c, and g_e being the volume fractions of the liquid, columnar, and equiaxed phases, ρ_l, ρ_c, and ρ_e the corresponding densities, and $\bar{C}_l$, $\bar{C}_c$, and $\bar{C}_e$, the corresponding species concentrations averaged over the RVE. Note that the volume fractions, densities, and averaged concentrations are supposed to be constant in the RVE but may vary with time. Mass and species variations must be consistent with the Divergence theorem applied to the RVE. In the case of gas bubble formation in the RVE and motion of gas bubbles in or out of the RVE, Eq. [1] must be completed by the corresponding terms for the gaseous phase.

As described in Reference 2, four basic mechanisms are responsible for a change of C_{mix} in the RVE. Note that the following description of the four mechanisms considers idealized scenarios. The fact that in reality a combination of different mechanisms may act simultaneously and/or successively will be discussed intensively in the next sections.

Type A: Macrosegregation Formation Associated with the Dynamic of Melt Flow.

- Inflow of enriched melt replacing depleted melt leads to an increase of C_{mix}. Thus, we term this mechanism Type A^+.
- Inflow of depleted melt replacing enriched melt leads to a decrease of C_{mix}. Thus, we term this mechanism Type A^-.

Type B: Macrosegregation Formation Associated with the Dynamic of Moving Crystals (Figure 1). Without loss of generality, it is assumed that the solute content of the solid is lower than that of the liquid ($k < 1$ with $k := C_s/C_l$ being the redistribution coefficient). If the opposite applies, the argumentations given below must be reversed.

- Outflow of crystals and the corresponding inflow of melt leads to an increase of C_{mix}. Thus, we term this mechanism Type B^+.
- Inflow of crystals and the corresponding outflow of melt leads to a decrease of C_{mix}. Thus, we term this mechanism Type B^-.

Type C: Macrosegregation Formation Associated with the Dynamic of a Compact Mush (Figure 2). By compact mush, we mean a rigid solid skeleton that either consists (i) of arrays of columnar dendrites at any columnar volume fraction or (ii) of globular/equiaxed crystals that exceeds the packing limit. As with Type B, it is assumed that $k < 1$ without loss of generality.

- Outward motion or widening of a compact mush and inflow of melt leads to an increase of C_{mix}. Thus, we term this mechanism Type C^+.
- Inward motion or compression of a compact mush and outward flow of melt leads to a decrease of C_{mix}. Thus, we term this mechanism Type C^-.

Type D: Macrosegregation Formation Associated with the Dynamic of Phase Transition (Figure 3). Without loss of generality, it is assumed that the solid reveals a higher density when compared with that of the liquid ($\rho_l < \rho_{c,e}$). If the opposite applies, the argumentations given below must be reversed.

- Inward flow of melt to compensate solidification shrinkage leads to an increase of C_{mix}. Thus, we term this mechanism Type D^+.

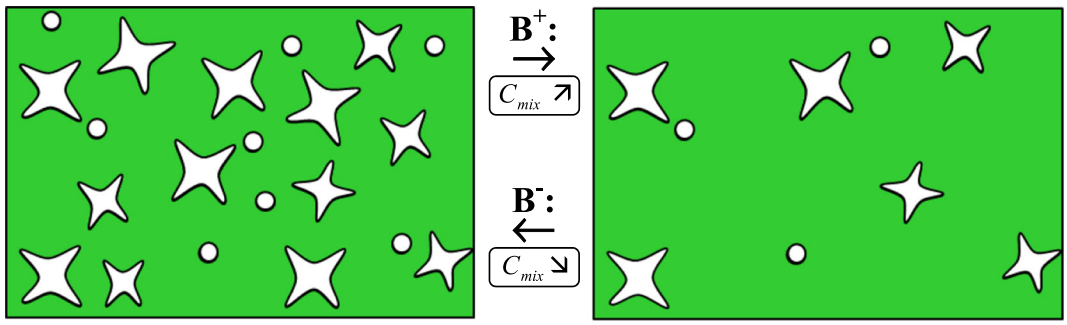

Fig. 1—Schematic illustration of the Type B mechanism. Crystals leaving the RVE cause an increase in C_{mix}; crystals entering the RVE cause a decrease.

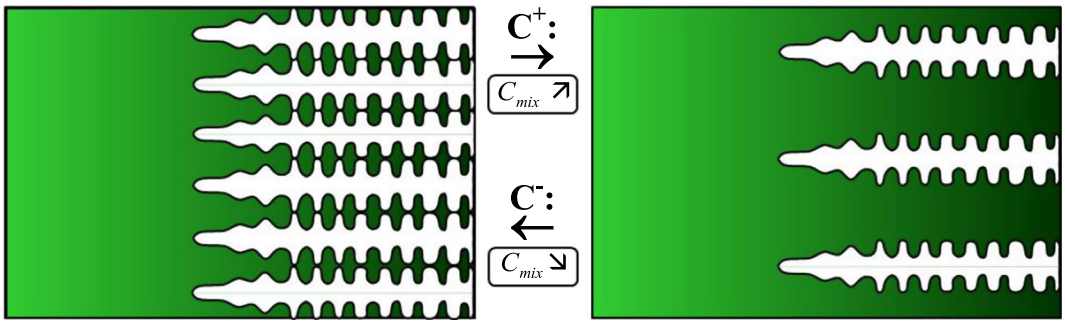

Fig. 2—Schematic illustration of the Type C mechanism. Outward motion or widening of a compact mush leads to an increase of C_{mix}; inward motion or compression of a compact mush leads to a decrease.

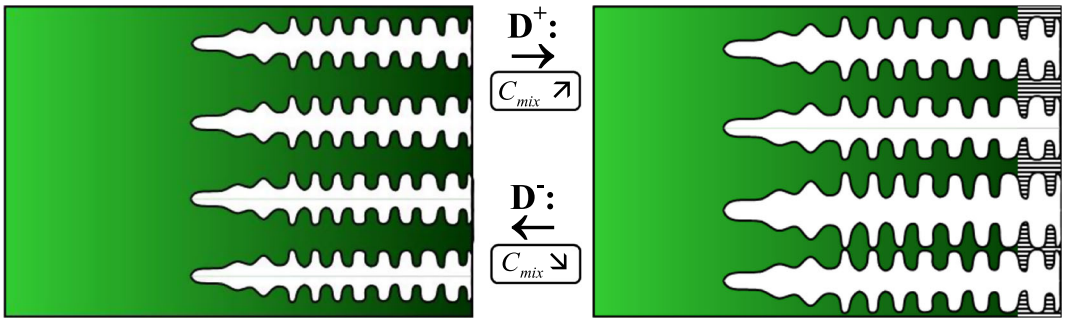

Fig. 3—Schematic illustration of the Type D mechanism. Inward flow of melt to compensate solidification shrinkage leads to an increase of C_{mix}; outward flow of melt caused by the volume expansion on melting melt leads to a decrease.

- Outward flow of melt caused by the volume expansion on melting leads to a decrease of C_{mix}. Thus, we term this mechanism Type D^-.

If the development and motion of gas bubbles during solidification would also be considered, a Type E mechanism could be defined.[13] However, this is beyond the scope of the present paper.

Note that the severity of each mechanism is highly material and process dependent (nucleation, solute redistribution coefficient, phases that occur and their morphologies, mush permeability, concentration- and/or temperature-dependent densities, *etc.*). Note further that when different mechanisms act they may equalize each other and so the mixture concentration in the RVE may not be changed.

B. *Combined Effects*

Generally, any combination of the types of basic macrosegregation formation might occur. It is the appraisal of the dominant types and their relative importance that makes the explanation of macrosegregation difficult. However, early work by Flemings *et al.*[5–7] showed that two special cases are quite important, namely segregation that forms close to a mold surface and segregation that forms due to the extending or shortening of a mushy zone.

C. *Evolution of Surface Segregation*

Consider the RVE in the melt being just adjacent to a (mold) surface. As in technical alloy nucleation, undercooling can be neglected, and solidification starts when the temperature drops below the liquidus temperature of the alloy. In this so-called chill zone, the first solid that forms reveals a dendritic morphology of multiple, fine-grained crystals which stick to the mold wall.[1] For the prevailing cases, where $\rho_s > \rho_l$ holds, the Type D^+ mechanism acts (inward flow of melt to compensate solidification shrinkage) and thus C_{mix} increases. Vaughan in Reference 14 stated $C_{mix} > C_0$ at casting surfaces "Inverse Surface Segregation" in order to distinguish it from the negative surface segregation known from the initial transition in zone melting (were solidification happens with a planar solid/liquid interface). Here, C_0 stands for the initial alloy composition.

Note that often forced melt flow (inlet flow, electromagnetic stirring, *etc.*) replaces segregated melt by less-segregated melt in the chill zone and so the Type A^- mechanism acts together with the formally discussed Type D^+ mechanism. This may reduce or even eliminate a positive segregation at the casting surface.

Also, in cases of losing the mechanical contact of the first crystals with the mold, they may simply slip downward and so the Type B^+ mechanism (outflow of crystals and the corresponding inflow of melt) acts and thus the positive surface segregation may even be amplified.

Freezing of aqueous solutions may be accompanied by the formation of negative surface segregation as in that case $\rho_s < \rho_l$ holds and the phenomenon reverses.

D. *Evolution of Segregation Due to Changes in the Mushy Zone Length*

Corresponding to the conditions employed on the definition of a RVE (see Section II–A), a mushy zone must be described with several RVEs where the volume fraction of liquid must be uniform on each individual RVE but decreases continuously from $g_l = 1$ to $g_l = 0$ along the mushy zone. Let us now consider three RVEs located at different positions, namely at the beginning of the mushy zone, somewhere at the center, and where solidification ends. For all three RVEs, compensation of solidification shrinkage must be ensured* and therefore the Type D^+ mechanism acts.

*In the present discussion formation of shrinkage porosity is neglected.

On the other hand, the compensation of solidification shrinkage also induces a melt flow along the mushy zone. The RVE at the beginning of the mushy zone feels thus a large inflow and outflow of melt, whereby the inflow is of C_0-composition and the outflow is already slightly segregated (due to solidification happening in this RVE). So, the Type A^- and Type D^+ mechanisms act simultaneously. It is obvious that due to the large inflow and outflow, the Type A^- mechanism prevails against the Type D^+ mechanism. Thus, for RVEs at the beginning of the mushy zone, C_{mix} decreases.

For an RVE somewhere at the mushy zone center, the same basic mechanisms act. However, the amount of inflow and outflow has decreased as now only a smaller volume has to be fed and so the severity of the Type A^- mechanism decreases. This decrease in severity of the Type A^- mechanism continues until it vanishes totally at the RVE where solidification ends. In fact, there is a position around the center of the mush where the decreasing severity of the Type A^- mechanism becomes equal to that of the Type D^+ mechanism. Until this very point C_{mix} decreases. With equalized severities, C_{mix} does neither decrease nor increase. For RVEs located deeper in the mush, the severity of the Type D^+ mechanism now prevails against that of the Type A^- mechanism and so C_{mix} increases. This increase continuous until the initial concentration is reached at the RVE where solidification ends and $C_{mix} = C_0$ is reached again.

Summarizing, the competition between Type A^- and Type D^+ mechanisms leads first to a continuous reduction of C_{mix} along the mushy zone, followed by a continuous increase until the initial concentration is reached again at the end of solidification. To the authors' knowledge, no analytic expression for the exact location of the C_{mix} minimum at the center of the mushy zone has yet been derived.

In Flemings' pioneering work,[5–7] the authors investigated what happens when the temperature gradient decreases and thus the mushy zone increases in length. This happens usually during solidification governed by mold cooling. In this case, the relative severity of the Type A^- and Type D^+ mechanisms is no longer balanced, whereby now the Type D^+ mechanism dominates. Thus, finally C_{mix} exceeds C_0 and a positively segregated solid is formed.

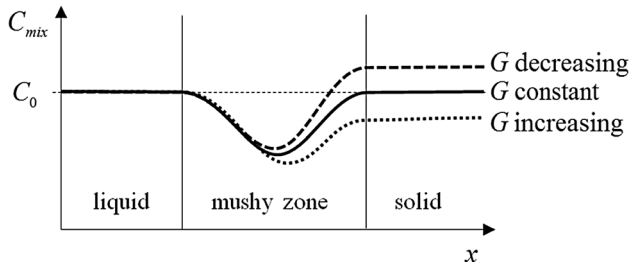

Fig. 4—Schematic illustration of C_{mix} along the mushy zone. For solidification with constant mushy zone length (constant temperature gradient), no macrosegregation forms, whereas for a mushy zone which increases its length (decreasing temperature gradient) a positively segregated solid is formed ($C_{mix} > C_0$) and for a mushy zone which decreases its length (increasing temperature gradient) a negatively segregated solid is formed ($C_{mix} < C_0$).

The opposite happens when the temperature gradient increases and thus the mushy zone decreases in length. In this case, the Type A^- mechanism prevails against the Type D^+ mechanism, and so C_{mix} does not increase to C_0 and so a negative macrosegregation forms. In Figure 4, these three cases, constant, increasing, and decreasing mushy zone length, and their implication on C_{mix} along the mushy zone are schematically illustrated.

III. INDUSTRIAL CASES

In the following, the four types of macrosegregation formation introduced above are applied to understand the formation of macrosegregation in (i) DC-casting of copper-based alloys; (ii) DC-casting of aluminum-based alloys; (iii) continuous casting of steel; and (iv) ingot casting of steel. In order to identify the basic mechanism responsible for the the formation of the corresponding macrosegregation, the flow which acts has to be identified first.

A. *DC-Casting of Copper-Based Alloys*

The most economical way to produce bronze alloys is vertical, semi-continuous casting: The melt is poured from a tundish directly into a cylindrical or rectangular mold *via* several inlet gates, and then pulled downward. After the strong heat extraction by the water-cooled mold (primary cooling) further cooling is achieved by spraying water directly onto the surface of the ingot (secondary cooling). The casting stops when the bottom of the pit is reached. After cutting off a certain length of the ingot, the process is started again. Figure 5 shows some typical macrosegregation profiles in Sn–bronze as published by the authors in Reference 15. Usually,

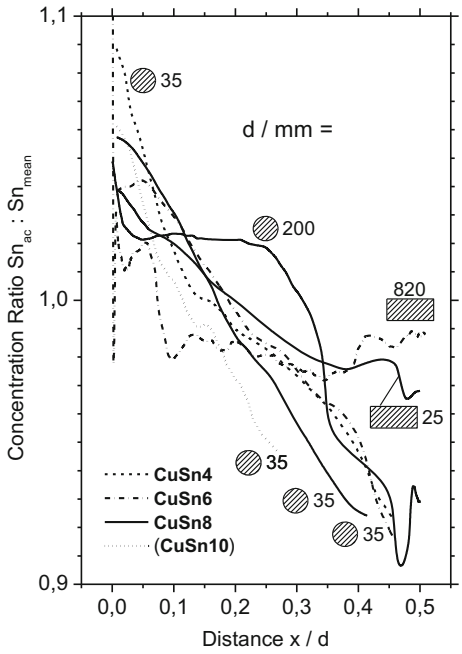

Fig. 5—Segregation curves across the Tin bronze ingots of cylindrical or rectangular shape with d being the dimension, x the position of chemical analysis measured from the surface, Sn_{mean} the mean Tin content of the ingot, and Sn_{ac} the actual Tin content at position x (taken from Ref. [15]).

positive macrosegregation is found at the billet surface and negative segregation in the billet center.

In order to elucidate the mechanism which leads to such typical macrosegregation profiles, several volume-averaging multiphase simulations had been performed by the authors. It turned out that considering a columnar phase growing from the mold wall inward and allowing the melt to flow through the permeable mushy zone driven by a solidification shrinkage-induced feeding flow are sufficient to explain the general shape of the macrosegregation profile.[15–17] It was also shown that the exact shape may be affected by forced inlet flow or thermo-solutal buoyancy flow. However, for a precise prediction on the impact these flow modes might have on the macrosegregation profile, the mushy zone permeability and the thermal and solutal expansion coefficients of the liquid must be known precisely.

Figure 6 shows the estimated C_{mix} pattern for an axis symmetrical continuous casting of an Sn–bronze alloy with red representing the largest values and blue the lowest. Green shows the initial concentration. On the right, a macrosegregation profile for Sn as typically measured is shown. The inverse surface segregation, originated by the Type D^+ mechanism (see Section II), is obvious in both the simulation and the experiment. The positively segregated outer areas are formed as the temperature gradient perpendicular to the billet decreases and the length of the mush increases. According to the explanation in Section II, this results in the formation of solids which are positively segregated. The C_{mix} pattern shown in Figure 6 shows the negatively segregated mush and the resulting (here only slightly) positively segregated solid, as explained in Section II.

When the dendritic solidification from the circumference of this cylindrical casting meets in the center, the negatively segregated mush merges. In addition, the relatively large center area is fed right from the bulk melt and thus the Type A^- mechanism is clearly prevailing over the Type D^+ mechanism. This leads to a strong negative C_{mix} in the center. Only when solidification at the centerline is about to be completed, the Type D^+ mechanism becomes stronger than Type A^- and thus C_{mix} increases again. However, this increase is only of minor importance and so a strong negative segregation at the center remains.

As shown in References 18 through 20, the same analysis on the formation of macrosegregation in semi-continuous casting of bronze holds for ternary alloys. However, the explanation given above does not consider the possible existence of equiaxed crystals in the center of the billet. In the case where equiaxed crystals form ahead of the growing columnar dendrites, they may sink downward along the columnar tip front and sediment at the center part of the billet. This would increase C_{mix} along the columnar tip region by the Type B^+ mechanism and decrease C_{mix} in the center part by the Type B^- mechanism. However, the relative severity of the corresponding changes in C_{mix} depends on the amount of equiaxed crystals, their size, morphology, and material density. If the conditions are such that the columnar dendrites stop growing (either by hard or soft blocking), the Columnar-to-Equiaxed Transition (CET) occurs. A approximate condition for this to happen is the increase in the volume fraction of the equiaxed crystal by 50 pct. On the other hand, equiaxed crystals may also form a "packed bed", that is a stacking of crystals where they are mechanically locked so that a rigid solid network occurs. This is believed to happen when their volume fraction exceeds a corresponding packing limit (such as 63.4 pct for spherical grains). A "packed bed" of equiaxed crystal is rather similar to an array of columnar dendrites: it may move with the casting velocity, continue to solidify, and may, to some extent, allow the residual melt to flow through. In Reference 21, the corresponding scenario had been modeled, whereby the conditions were chosen such that half of the billet was assumed to solidify with equiaxed crystals. It turned out that the corresponding macrosegregation profile is quite similar to the one without considering the equiaxed crystals. However, two possible differences are discussed in Reference 21. Firstly, if close to the CET the permeability of the columnar array differs from that of the equiaxed crystals, the interdendritic flow may choose the easier path which then leads to a "trace" in the macrosegregation profile. Secondly, vortices induced by the downward sliding of the equiaxed crystals may also lead to a local variation in C_{mix} at the equiaxed regions. This may explain the W-type shape of the macrosegregation profile sometimes observed in the center of a bronze billet.

B. *DC-Casting of Aluminum-Based Alloys*

DC-casting of aluminum-based alloys is comparable with the DC-casting of bronze (Figure 7(a)). The two main differences are as follows: First, aluminum-based

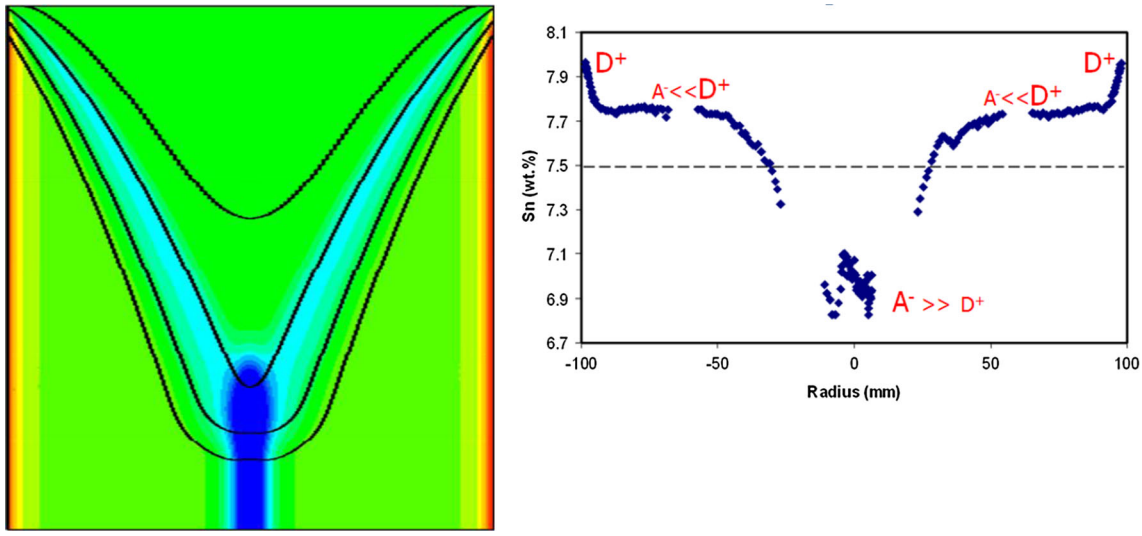

Fig. 6—Left: Simulated distribution of the mixture concentration for an axis symmetrical continuous casting process of bronze. The positive inverse surface segregation is shown in red. Green shows the initial concentration and light/dark blue the negatively segregated areas. Liquid fraction isolines are shown for g_l = 0.01, 0.5, 0.7, and 0.9. Right: Typical measured macrosegregation profile (taken from Ref. [16]) and types of basic mechanisms responsible for macrosegregation formation. Explanations are given in the text (Color figure online).

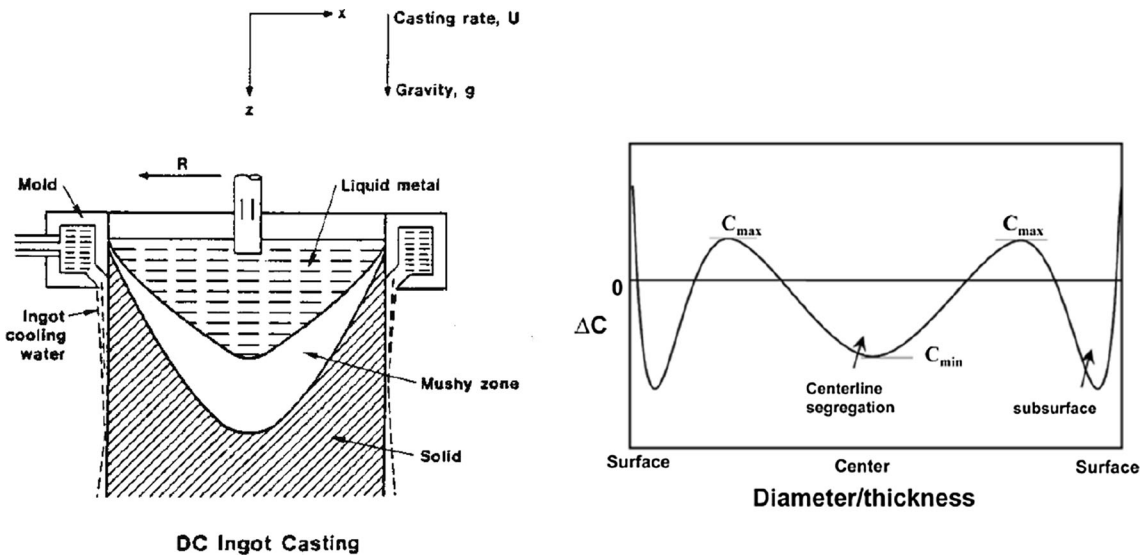

Fig. 7—Process schema (left) and typical segregation profile (right) for DC-casting of aluminum-based alloys (taken from Ref. [3]).

alloys are usually cast with some amount of grain refiners. Therefore, solidification happens by the formation of equiaxed crystals. At low solid fraction, the equiaxed crystals are able to move, whereas for high solid fraction they form a rigid network. The transition is thought to happen at the coherency temperature which might coincide according to Reference 3 with a volume fraction of around 30 pct for most aluminum-based alloys. The area where the equiaxed crystals are able to move is called a slurry, whereas the area where they form a rigid network is called a mush. Both together form the mushy zone.

Second, many aluminum-based alloys show a significant thermal contraction of the solidifying shell, so that a gap between the mold and the billet surface forms. This gap drastically reduces the heat transfer. In consequence, the heat from the bulk melt increases the shell temperature again and so partial remelting occurs. The heat transfer is again increased when the secondary cooling is reached.

These two differences between DC-casting of copper- and aluminum-based alloys have a drastic impact on the formation of macrosegregation. Figure 7(b) shows a typical segregation profile for aluminum-based alloys. The main difference to the segregation profile in bronze alloys (Figure 5) is the fact that the profile for aluminum-based alloys reveals negatively segregated areas close to the positive inverse surface segregation.

In order to elucidate the reason why these negatively segregated areas form, let us first discuss the impact of

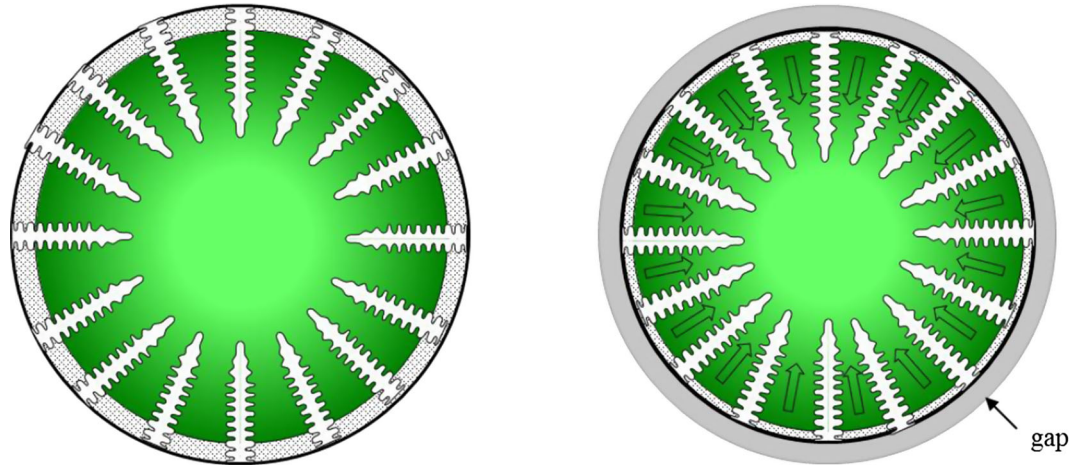

Fig. 8—Schematic diagram of a cross section of a round DC-casted billet of an aluminum-based alloy showing the compression of the mushy zone in the area where a gap between mold and solidifying billet forms. Left: Cross section of a billet before gap formation. Right: Cross section of a billet after gap formation. The gap is shown as a gray ring.

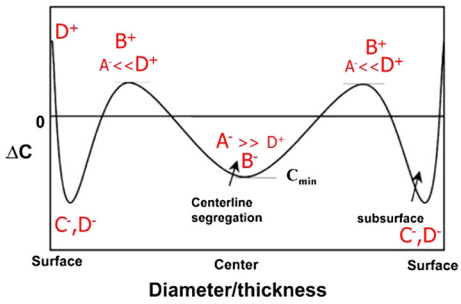

Fig. 9—Types of basic mechanisms responsible for a typical macrosegregation profile often found in DC-casting aluminum-based alloys. Explanations are given in the text.

equiaxed solidification on the macrosegregation profile. Without motion of equiaxed crystals, solidification-induced feeding flow would lead to a segregation profile similar to that for bronze alloys. Namely positive surface segregation by Type D^+, a positive segregated solid as long as the mushy zone increases its length by Type $D^+ \gg A^-$ and finally a negatively segregated core due to feeding with bulk melt by Type $A^- \gg D^+$ (Figure 6). The phenomena discussed for bronze alloys are similarly occurring for the equiaxed mush below the coherency temperature. The same is true for the slurry above the coherency temperature. However, now the motion of equiaxed crystals has to be taken into account too. As the equiaxed crystals in the slurry generally move downward along the coherency limit, we would expect that a Type B^+ mechanism acts close to the billet surface and a Type B^- mechanism where the equiaxed crystals finally settle, namely at the center. Obviously, the motion of the equiaxed crystals in the slurry zone intensifies the segregation tendency already given by solidification-induced feeding flow and is thus not the intrinsic reason for the negatively segregated areas being close to the positively segregated surface areas.

As mentioned above, thermal contraction of the solidifying shell leads to gap formation and thus to an increased temperature in the shell/mushy zone region. If an RVE would be located close to the surface of the billet, it would feel compression of the solid skeleton which gives rise to the Type C^- mechanism (inwards motion or compression of a compact mush) and partly remelting of the solid skeleton which gives rise to the Type D^- mechanism (outwards flow of melt caused by the volume expansion on melting melt). Figure 8 shows this schematically. Obviously, compression and remelting both result in a decrease of C_{mix} and thus result in formation of the negatively segregated areas close to the positively segregated surface area.

However, the authors have to admit that they are not aware of any simulation efforts which can prove this statement. Simulations of flow, dendritic solidification, and compression of the solidified shell are still tasks which can be fulfilled only in parts. Instead, there exists simulation results of solidification of the equiaxed aluminum-based alloys that also take thermo-solutal buoyancy flow into account.[22–25] Similar to the simulations of columnar solidification of bronze considering also thermo-solutal buoyancy,[16] the induced flow can be such that less-segregated melt may be transported from the bulk melt to a position close to the surface and so negative segregations may form there too. However, it is also shown in Reference 16 that those predictions depend highly on the assumed mushy zone permeability. With lower permeability, the effect of thermo-solutal buoyancy becomes less pronounced. Unfortunately, mushy zone permeabilities are not known with the necessary accuracy.

In Figure 9, the different reasons for typical segregation profiles in aluminum-based alloys are gathered including the impact compression and local remelting might have.

C. *Continuous Casting of Steel*

Industrial practice has shown that macrosegregation can also be found in continuously cast steel strands. A typical segregation profile often observed is shown in Figure 10 with a positively segregated peak at the

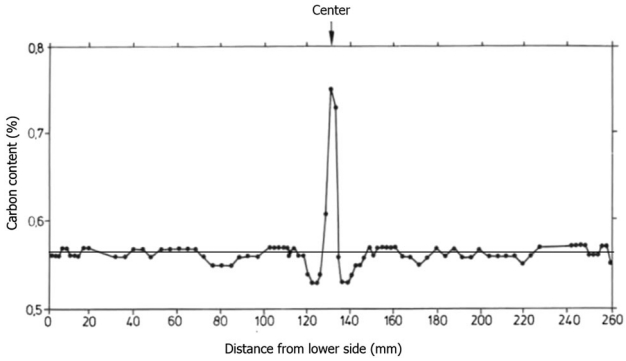

Fig. 10—Typical segregation profile across a continuous cast steel slab (taken from Ref. [26]).

centerline and a negatively segregated minima at both sides. Miyazawa and Schwerdtfeger[26] were the first to demonstrate that such a profile is a result of bulging of the solid shell between the rolls in continuous casting machines. Kajitani *et al.*[27] had adapted his approach, whereby they approximately modeled both deformation of the solid shell and interdendritic flow between five successive rolls. Fachinotti *et al.*[28] and Bellet[29] modeled the bulging phenomena with a more sophisticated viscoplastic model, as solid steels at elevated temperatures might reveal a negligible small static plasticity threshold and very weak stresses generate deformation by creep.

In recent years, the group of the authors simulated solidification of a full strand with a corresponding Eulerian–Eulerian volume-averaging approach that considers solidification-induced feeding flow and bulging between 101 rolls. It was shown that bulging is indeed a necessary condition to produce positive centerline segregation. In Reference 30, it was demonstrated that without bulging even in steel negative centerline segregation will form by similar mechanisms to what has been described in Sections III–A. Compared to this, bulging of the hot solid shell between each pair of guiding rolls successively increases C_{mix} along the centerline and decreases C_{mix} beside the centerline (Figure 11).[31,32] This happens as soon as the strand center reveals some dendritic network, which is then moving outward and inward with the bulging solid shell. As solidification proceeds, the inward motion is accompanied by some deformation of the dendritic network.

It is shown in Reference 32 that solidification-induced feeding can reduce the strength of positive centerline segregation caused by bulging by *e.g.*, 50 pct (Figure 11). However, the resulting effect of solidification-induced feeding flow (negative centerline segregating) and bulging-induced flow (positive centerline segregating) depends on various factors such as density difference between liquid and solid, phase diagram details, mechanical properties of the solidifying shell, cooling and geometrical aspects, *etc.* and it is quantitatively difficult to predict the effect.

In order to understand the mechanisms which lead to the periodical increase of C_{mix} along the centerline and decrease along both sides, let us consider continuous casting with bulging between each different pair of rolls but neglecting solidification-induced feeding flow. Due to the inward and outward motion of the dendritic network, the mechanism which governs the formation of macrosegregation is of Type C. For an RVE moving with the casting speed along the centerline, we have a continuous outward and inward motion of dendritic network compensated by melt flow against the casting direction mainly along the centerline. That is why alternatively Type C^+ (outward motion in region A in Figure 12) and Type C^- (inward motion in region B in Figure 12) mechanisms act. Without any solidification, the effect of both mechanisms would simply compensate and C_{mix} would oscillate but remain on an equal level. The net increase of C_{mix} at the centerline is caused by the fact that the Type C^+ mechanism prevails against the Type C^- mechanism, and that is because solidification has increased the average solute concentration of melt which flows from region B to region A.

For the areas on both sides of the centerline, again Type C^+ and Type C^- mechanisms occur alternatly. However, the melt in the corresponding RVEs flows through from their closest neighborhood. So Type A^+ acts for an RVE in the upper areas of region A and Type A^- for the RVE in the upper areas of region B. The net result is that the increase of C_{mix} in the upper parts of region A is less strong than the decrease in the upper parts of region B.

As is known from industrial practice, centerline segregation in continuously solidifying strands can be reduced by mechanical soft reduction. Based on an Eulerian–Eulerian two-phase volume-averaging approach, the group of the authors published a couple of investigations on intrinsic phenomena happening when mechanical softreduction is applied.[33–37]

D. *Ingot Casting of Steel*

Most of the empirical knowledge on macrosegregation in steel ingots was built early in the last century.[38–44] As full-scale trials were (and still are) extremely costly, the first theoretical models on the formation of macrosegregation in ingots were suggested by Hultgren,[45] Oeters *et al.*,[46] Chuang and Schwerdtfeger,[47] den Hartog *et al.*,[48] Flemings,[44] and Fredriksson.[49] The typical segregation pattern in a steel ingot consists of positive segregation in the upper region, a conical negative segregation in the lower region, 'V'-segregations along the centerline, and 'A'-segregations in the middle radius region between the casting outer surface and the centerline[43,44,50] (Figure 13).

Since the early numerical modeling attempt by Flemings *et al.*,[51,52] several macrosegregation simulations for ingot casting have been developed.[53–56] Gu and Beckermann[56] were the first to apply a coupled multicomponent solidification model with melt convection to a large industry-scale ingot. Their simulation qualitatively agreed with the positive segregation observed in the upper region of the ingot. However, because the sedimentation of free equiaxed crystals was neglected, they could not properly predict the negative segregation at the lower region of the ingot. Combeau *et al.*[57,58] presented a two-

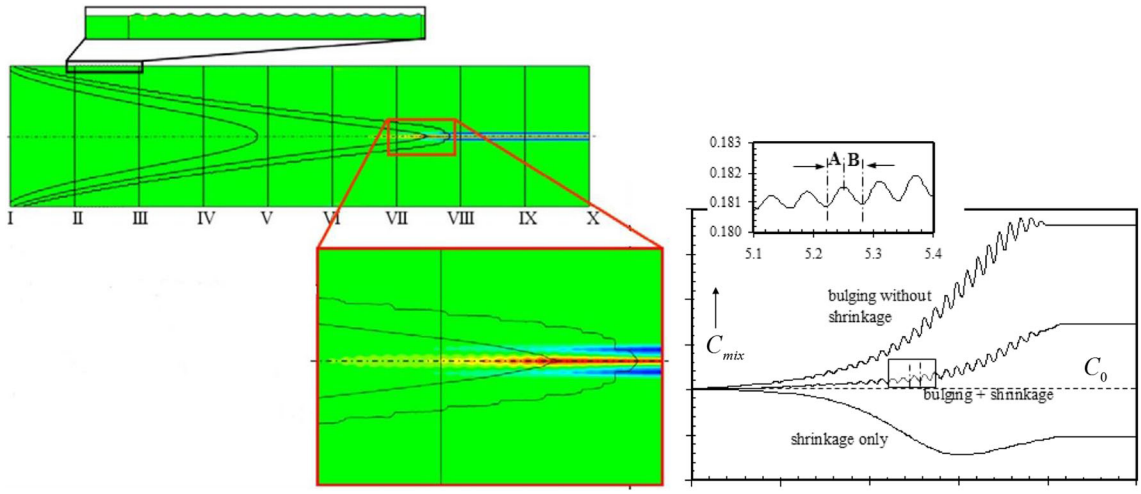

Fig. 11—(Left) Predicted macrosegregation in terms of C_{mix} (red: high, blue: low, green: initial value) in a horizontal model steel slab taking only bulging into account (length scaled 1:10). Volume fraction isolines for g_s = 0.01, 0.5, and 0.8 are also shown. (Right) Comparison of centerline segregation for three different cases corresponding to solidification of the horizontal model steel slab: (i) shrinkage only, (ii) bulging only, and (iii) combined effect of shrinkage and bulging. (taken from Ref. [32]) (Color figure online).

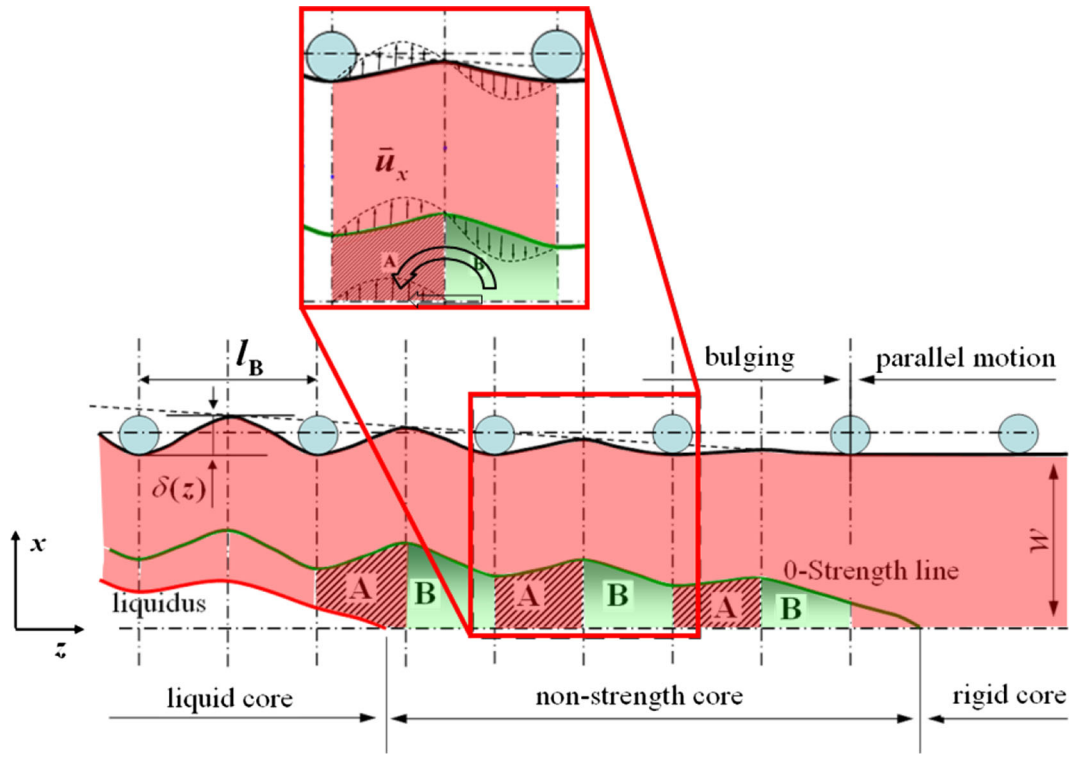

Fig. 12—Schematic of solid motion with a series of bulging rolls (taken from Ref. [32]) (Color figure online).

phase model to study the influences of both motion and morphology of equiaxed grains on a 3.3-ton steel ingot. Some progress was made toward predicting the behavior at the negative segregation zone in the lower region of the ingot. However, these researchers did not distinguish the columnar phase from the equiaxed phase, both of which are present and interact with each other during solidification. The team of authors[59,60] developed a mixed columnar-equiaxed solidification model which directly accounts for nucleation and growth of equiaxed globular grains, growth of columnar dendrite trunks, and both equiaxed grain sedimentation and melt convection. Their studies successfully predicted both the conical negative segregation in the lower region of the ingot and the columnar-to-equiaxed transition (CET). In Reference 61 they applied their model to study macrosegregation in a 2.45-ton, large-end-up, industry steel ingot that was reported in the literature.[38]

In the following, we take results from the studies on that 2.45-ton ingot to demonstrate how the appearing

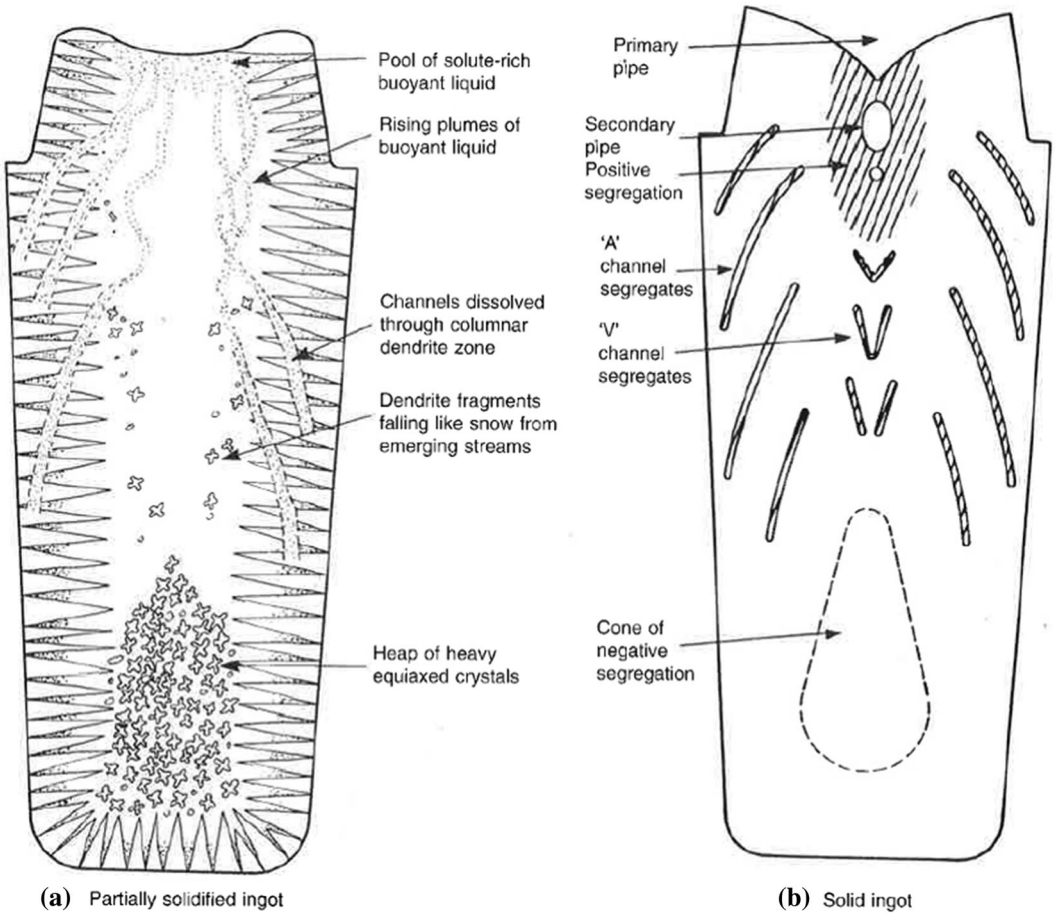

Fig. 13—Development of segregation in a killed steel ingot (*a*) during solidification and (*b*) in the final ingot (taken from Ref. [50]).

macrosegregation in steel ingots can be linked to the basic mechanisms. In Figures 14(a) through (f) six different stages of the solidification process of such an ingot are shown, whereby each time (i) the equiaxed volume fraction; (ii) the velocity of equiaxed crystals; (iii) the columnar volume fraction; (iv) the liquid velocity; and (v) the mixture concentration, C_{mix}, are presented. Although, the shown process details are already complex, solidification-induced feeding flow and deformation of the ingot were neglected in this simulation. That's why Type C and Type D mechanisms are not considered and their impact on macrosegregation for ingot casting is not discussed here.

The process conditions for this simulation were chosen such that (i) cooling from the ingot top is slower compared to cooling from the sides and the bottom as to mimic 'hot toping'; (ii) nucleation happens in undercooled areas mostly ahead of the columnar front; (iii) equiaxed crystals may sediment due to a larger material density compared to the melt; (iv) thermo-solutal buoyancy is accounted for; (v) equiaxed crystals are captured in the columnar array if the volume fraction of columnar crystals is larger than 20 pct; (vi) captured equiaxed crystals continue to grow as equiaxed crystals (they do not transfer to become columnar); (vii) equiaxed crystals become immobile when their volume fraction exceeds 64 pct; (viii) the columnar front stops growing when the volume fraction of equiaxed crystals exceeds 50 pct (hard blocking, soft blocking is automatically accounted for); (ix) the ingot is axis symmetrical.

Under these conditions, solidification starts along the mold walls and at the bottom by forming a columnar solidification front in combination with a small amount of equiaxed crystals (Figure 14(a)). In addition, thermal buoyancy leads to a downward motion of liquid along the walls and an upward motion of the melt flow at the center. Equiaxed crystals being dragged by the liquid (and also owing to its own weight) move downward along the columnar front and sediment mostly at the bottom area. Only a small amount of equiaxed crystals is temporarily moving slightly upward following the liquid by drag. In addition to the scenario described here, cooling at the ingot top also leads to a thermally driven downward motion of melt along the ingot center. So, in the lower part of the ingot, the melt rises along the center, whereas at the upper part of the ingot the melt sinks along the center. The image given in Figure 14(a) was taken just before these two melt flows met.

At this stage of solidification already some C_{mix} deviations have formed. A slightly negatively segregated area at the bottom forms due to sedimentation of crystals, that is by the Type B^- mechanism. The sedimented crystals which originally formed somewhere

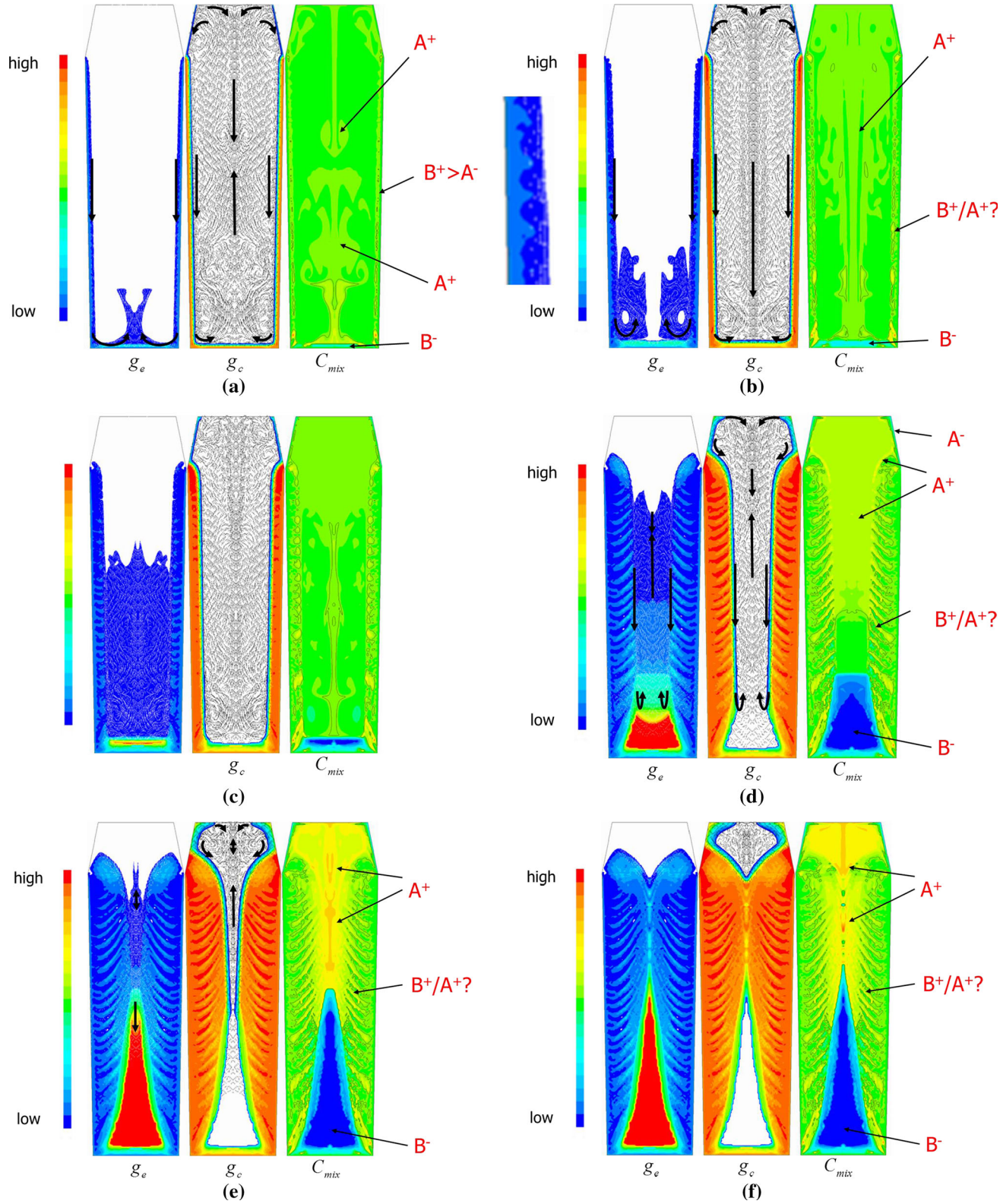

Fig. 14—Multiphase simulation of solidification of a 2.45-ton steel ingot. Left: equiaxed fraction and equiaxed velocity; middle: columnar fraction and liquid velocity; right: mixture concentration (simulation presented in Ref. [61]) (*a*) $t = 2$ min, (*b*) $t = 5$ min, (*c*) $t = 12$ min, (*d*) $t = 32$ min, (*e*) $t = 52$ min, (*f*) $t = 76$ min (Color figure online).

along the columnar front were partly replaced by other sinking crystals. The parts which are not replaced is leading to the formation of positively segregated areas along the columnar front by the Type B^+ mechanism. In addition, the thermally induced streams along the columnar front washes segregated melt out of the mush

and transports it into the bulk melt. That is why the Type A^- mechanism acts along the mush and the Type A^+ mechanism leads to an increase in C_{mix} at the ingot center as indicated in Figure 14(a).

Following the dynamics of the process, it turned out that the downward stream along the center from the top is at first stronger than the upward stream along the center from the bottom, and so the downward stream reaches the bottom of the ingot (Figure 14(b)). In fact, the downward flow along the columnar front caused by both thermal buoyancy and drag of sinking equiaxed crystals and the corresponding upward flow along the center from the bottom continue during the whole solidification process. This is also true for the thermally induced downward flow along the center from the ingot top. As can be seen in Figures 14(c) through (f), the stagnation point of these two opposed streams is gradually moving upward while oscillating irregularly back and forward.

During the whole course of the solidification process, the equiaxed crystals continue to nucleate and sink along the columnar front. In the sedimented bed at the lower part of the ingot, the amount of equiaxed crystals quickly exceeds 50 pct so that the columnar front is stopped and CET happens. Within this cone of equiaxed crystals, negative macrosegregation is established by the Type B^- mechanism (see blue cone in Figures 14(c) through (f)). Also the transport of segregated melt from the different mushy zone areas continues during the whole course of the solidification process. This leads to a gradual increase of C_{mix} in the residual melt by the Type A^+ mechanism (Figures 14(c) through (f)).

Quite important is the fact that right from the beginning the capturing of equiaxed crystals into the columnar front is uneven. In the left insert in Figure 14(b), it can be seen that the captured equiaxed crystals start to reveal an oscillatory pattern. The origin of the characteristic length scale for this oscillatory pattern is at present the subject of discussions and further investigations. Following the further dynamics of the solidification process reveals that this oscillatory variation in the amount of captured equiaxed crystals continue and becomes even stronger (see Figures 14(c) through (f)). Note that the total amount of solid which locally forms is governed by heat extraction and does not show any oscillatory pattern. That is why the columnar phase reveals the opposite volume fraction oscillation as the equiaxed one. It is also important to mention that the resulting 'finger' of higher amount of equiaxed crystals turn toward the downward flow and thus 'bend' upwards—similar to dendrites growing toward the given flow direction. And it is even more important that C_{mix} reveals a similar oscillatory pattern as the equiaxed and columnar phases. Obviously, those oscillatory patterns reveal some similarity with the classical 'A'-segregation. That is why we have termed them quasi 'A'-segregation. Up to now 'A' segregations were thought to be formed by localized channel flow in the mushy zone leading to the so-called freckles.[2,50,62–65] However, in the presented simulations, the underlying numerical grid is not fine enough to resolve a localized channel flow in the mushy zone and Figures 14(c) through (f) does not show any indication of that. This surprising finding leads us to a detailed study on the formation of these quasi 'A' segregations. In Reference 61 we have presented the corresponding results. It turned out that (i) the number density of quasi 'A' segregation increases with the increasing grid fineness, and (ii) quasi 'A' segregation also forms without any equiaxed crystals—they are obviously not caused by the interplay between equiaxed, columnar, and liquid phase. However, with equiaxed crystals, the severity of the quasi 'A' segregation increases by a factor of four.

Another important phenomenon can be observed when the columnar front from the mold wall meets at the ingot center (Figures 14(e) through (f)). Note that as long as the columnar dendrites do not meet at the center, equiaxed crystals that are still sinking downwards contributing to the negative cone. However, the moment the total solid volume fraction right at the center exceeds 64 pct, the motion of the solid is 'frozen in'. This is sometimes called 'bridging'. The equiaxed crystals from higher regions are still continuing to sink downward, however this downward sinking is unsteady as the stagnation point at the center is still oscillating. As a result, a sedimentation pattern of equiaxed crystals similar to a 'V' forms which is accompanied by negative segregation due to the Type B^- mechanism. So again, a way of forming 'V' segregations at the ingot center is found without resolving the individual flow channels. Just to be cautious we have called them quasi 'V' segregations.

Especially interesting are the processes happening in the area of 'hot toping'. By assuming reduced heat transfer, solidification is retarded and mostly columnar growth occurs (Figures 14(c) and (d)). Thermal buoyancy leads to a downward flow along the columnar front (in addition to the center) and thus a negatively segregated shell forms directly at the ingot surface by the Type A^- mechanism. Hereby, the washed away solute leads to an enriched melt which sinks down and is redirected by meeting the thicker solid shell at the kink of the ingot (Figure 14(d)).

IV. CONCLUSIONS

In recent years, numerical simulations on the description of metal-producing processes have become more and more sophisticated.[66] Especially, simulation of complex process details which leads to the formation of macrosegregation had been increasingly published. Although it has long been known that four basic mechanisms are responsible for the formation of macrosegregation, numerical simulations seldomly link the predicted macrosegregation with those basic mechanisms. The reason for this is that often complex and time-dependent processes occur during macrosegregation. Nevertheless, it is still worthwhile to name the basic mechanisms which are responsible for the occurrence of macrosegregation especially when the basic mechanisms act in combination with each other.

The four basic mechanisms are (i) solute redistribution caused by the melt dynamic (Type A), (ii) solute redistribution caused by the dynamic of equiaxed crystals (Type B), (iii) solute redistribution caused by

the dynamic of solid skeletons (Type C), and (iv) solute redistribution caused by the dynamic of phase transition (Type D). Principally, these mechanisms can result in the decrease or increase of C_{mix}. The severity of a mechanism might depend on the process and the material parameters such as phase diagram details, morphological details, mushy zone permeability, strength and plasticity of solid skeletons, *etc*.

The typical macrosegregation profile in columnar solidifying bronze billets can be understood by the Type A and D mechanisms. Inverse surface segregation is caused by Type D^+ and the positively segregated outer areas of billets by the fact that Type D^+ prevails against Type A^-. In the negatively segregated center, the relative severity of the mechanism reverses and now Type A^- prevails against Type D^+. The possible occurrence of the equiaxed crystals may enhance the positively and negatively segregated areas by Type B^+ and Type B^- mechanisms.

The arguments are similar for the interpretation of a segregation profile of billets made from (grain refined) the aluminum-based alloys. Here, the effect of the Type B mechanism might be stronger. However, the negatively segregated area close to the billet surface cannot be explained by grain motion. Rather, it is most probably caused by compression and remelting due to the formation of an air gap, and that is by Type C^- and D^- mechanisms.

Without successive bulging of the solidified shell centerline, segregation in steel strands would be negative caused by a similar mechanism as discussed for bronze billets. However, successive bulging leads to a repeated opening and closing of the centerline area which leads to the formation of dendritic strand cores by Type C mechanisms , and then to a net increase of C_{mix} right at the centerline and a net decrease of C_{mix} on both sides. The resulting positive centerline segregation will of course be weakened by the solidification-induced feeding flow and the resulting phenomena as they occur during DC-casting of copper-based alloys.

In ingot casting, it is clear that the negatively segregated cone is caused by the sedimentation of the equiaxed crystals following the Type B^- mechanism. Thermal buoyancy often lead to a downward motion along the ingot walls. This flow is responsible for the wash out of the solute from any mush and an enrichment of the bulk melt (Type A^+), namely the last melt to solidify. Besides this standard knowledge, quasi 'A' segregation in the bulk ingot and quasi 'V' segregation at the ingot center were predicted without resolving the individual flow channels in the mushy zone. Obviously, the process reveals a type of macroscopic instability which leads to those segregation patterns. Here further research is needed.

ACKNOWLEDGMENTS

This report is based on a plenary talk given at the 4th Int. Conf. on Advances in Solidification Processes (ICASP-4), July 2014 in Beaumont, Old Winsor, UK. The authors are grateful to the conference chairmen for being invited and getting the opportunity to present this overview on macrosegregation. We further acknowledge the financial support provided by the Austrian Federal Ministry of Economy, Family and Youth and the National Foundation for Research, Technology and Development within the framework of the Christian Doppler Laboratory for Advanced Process Simulation of Solidification and Melting. In addition, we acknowledge the cooperation of J. Domitner, F. Mayer, M. Grasser, and J. Li, J. Hao in various projects.

REFERENCES

1. W. Kurz and D.J. Fisher: *Fundamental of Solidification*, 4th ed., Trans Tech Publications, Aedermansdorf, 1998.
2. J.A. Dantzig and M. Rappaz: *Solidification*, EPFL, London, 2009.
3. R. Nadella, D.G. Eskin, Q. Du, and L. Katgerman: *Prog. Mater. Sci.*, 2008, vol. 53, pp. 421–80.
4. J.S. Kirkaldy and W.V. Youdelis: *Trans. Metall. Soc. AIME*, 1958, vol. 212, pp. 833–40.
5. M.C. Flemings and G.E. Nereo: *Trans. Metall. Soc. AIME*, 1967, vol. 239, pp. 1449–61.
6. M.C. Flemings, R. Mehrabian, and G.E. Nereo: *Trans. Metall. Soc. AIME*, 1968, vol. 242, pp. 41–49.
7. M.C. Flemings and G.E. Nereo: *Trans. Metall. Soc. AIME*, 1968, vol. 242, pp. 50–55.
8. C. Beckermann: *Flemings Symp. Boston, MA*, 2000.
9. G.H. Gulliver: *Metallic Alloys*, Griffin, 1922.
10. E. Scheil: *Z. Für Met.*, 1942, vol. 34, pp. 70–72.
11. H.D. Brody and M.C. Flemings: *Trans. Metall. Soc. AIME*, 1966, vol. 236, p. 615.
12. T.W. Clyne and W. Kurz: *Metall. Trans. A*, 1981, vol. 12A, p. 965.
13. A. Roosz: Personal Communication, 2014.
14. N.B. Vaughan: *J. Inst. Met.*, 1937, vol. 61, p. 35.
15. M. Gruber-Pretzler, F. Mayer, M. Wu, A. Ludwig, J. Riedle, and U. Hofmann: in *6th Int. Copper-Cobre Conf., (Cu2007), Vol 1*, Toronto, 2007, pp. 265–79.
16. A. Ludwig, M. Gruber-Pretzler, M. Wu, A. Kuhn, and J. Riedle: *Fluid Dyn. Mater. Process.*, 2005, vol. 1, pp. 285–300.
17. M. Gruber-Pretzler, F. Mayer, M. Wu, A. Ludwig, H.A. Kuhn, and J. Riedle: in *6th Int. Conf. Model. Cast. Weld. Adv. Solidif. Process. (MCWASP VI)*, C.A. Gandin and M. Bellet, eds., TMS Publication, Warrendale, 2006, pp. 799–806.
18. A. Ludwig, M. Gruber-Pretzler, F. Mayer, A. Ishmurzin, and M. Wu: *Mater. Sci. Eng. A*, 2005, vols. 413–4, pp. 485–89.
19. A. Ishmurzin, M. Gruber-Pretzler, F. Mayer, M. Wu, and A. Ludwig: *Int. J. Mater. Res.*, 2008, vol. 99, pp. 618–25.
20. J. Hao, M. Grasser, M. Wu, and A. Ludwig: *Adv. Mater. Res.*, 2011, vol. 155, pp. 1401–04.
21. J. Hao, M. Grasser, M. Wu, A. Ludwig, J. Riedle, and R. Eberle: *IOP Conf. Ser. Mater. Sci. Eng.*, 2012, vol. 27, p. 012015.
22. D.G. Eskin, J. Zuidema, V.I. Savran, and L. Katgerman: *Mater. Sci. Eng. A*, 2004, vol. 384, pp. 232–44.
23. Q. Du, D.G. Eskin, and L. Katgerman: *Mater. Sci. Eng. A*, 2005, vols. 413–414, pp. 144–50.
24. R. Nadella, D.G. Eskin, and L. Katgerman: *Metall. Mater. Trans. A*, 2007, vol. 39A, pp. 450–61.
25. D.G. Eskin, Q. Du, and L. Katgerman: *Metall. Mater. Trans. A*, 2008, vol. 39A, pp. 1206–12.
26. K. Miyazawa and K. Schwerdtfeger: *Arch. Eisenhüttenwes.*, 1981, vol. 52, pp. 415–22.
27. T. Kajitani, J. Drezet, and M. Rappaz: *Metall. Mater. Trans. A*, 2001, vol. 32A, pp. 1479–91.
28. V. Fachinotti, S. Le Corre, N. Triolet, M. Bobadilla, and M. Bellet: *Int. J. Numer. Methods Eng.*, 2006, vol. 67, pp. 1341–84.
29. M. Bellet: in *9th Int. Conf. Numer. Methods Ind. Form. Process.*, J.M.A. Cesar de Sa and A.D. Santos, eds., American Institute of Physics, Porto, 2007, pp. 1369–74.
30. F. Mayer, L. Könözsy, M. Wu, and A. Ludwig: in *2nd Int. Conf. Simul. Model. Met. Process. Steelmak. (STEELSIM 2007)*, A. Ludwig, ed., ASMET, Graz, 2007, pp. 265–70.

31. F. Mayer, M. Wu, and A. Ludwig: in *12th Int. Conf. Model. Cast. Welding, Adv. Solidif. Process. (MWASP XII)*, S.L. Cockcroft and D.M. Maijer, eds., TMS Publication, Vancouver, 2009, pp. 279–86.
32. F. Mayer, M. Wu, and A. Ludwig: *Steel Res. Int*., 2010, vol. 81, pp. 660–67.
33. M. Wu, J. Domitner, and A. Ludwig: *Metall. Mater. Trans. A*, 2012, vol. 43A, pp. 945–64.
34. J. Domitner, M. Wu, F. Mayer, A. Ludwig, B. Kaufmann, J. Reiter, and T. Schaden: in *Eur. Contin. Cast. Conf. (ECCC 2011)*, Düsseldorf, 2011, pp. S6.1–S6.8.
35. M. Wu, J. Domitner, F. Mayer, and A. Ludwig: in *4th. Int. Conf. Simul. Model. Met. Process. Steelmak. (STEELSIM 2011)*, 2011, pp. 1–11.
36. J. Domitner, M. Wu, A. Kharicha, A. Ludwig, B. Kaufmann, J. Reiter, and T. Schaden: *Metall. Mater. Trans. A*, 2013, vol. 45A, pp. 1415–34.
37. J. Domitner, M. Wu, and A. Ludwig: *Steel Res. Int*., 2014, vol. 85, pp. 1–5.
38. Iron and Steel Institute (London): *J. Iron Steel Inst*., 1926, vol. 113, pp. 39–176.
39. A. Hultgren: *J. Iron Steel Inst*., 1929, vol. 120, pp. 69–125.
40. E. Marburg: *J. Met*., 1953, vol. 5, pp. 157–72.
41. B. Gray: *J. Iron Steel Inst*., 1956, vol. 182, pp. 366–74.
42. C. Roques, P. Martin, Ch. Dubois, and P. Bastien: *Rev. Met*., 1960, vol. 57, pp. 1091–1103.
43. M.C. Flemings: *Metall. Trans*., 1974, vol. 5, pp. 2121–34.
44. M.C. Flemings: *Scand. J. Met*., 1976, vol. 5, pp. 1–15.
45. A. Hultgren: *Scand. J. Met*., 1973, vol. 2, pp. 217–27.
46. G. Ebneth, W. Haumann, K. Rüttiger, and F. Oeters: *Arch. Eisenhüttenwes*., 1974, vol. 45, pp. 353–59.
47. Y.-K. Chuang and K. Schwerdtfeger: *Arch. Eisenhüttenwes*., 1975, vol. 46, pp. 303–10.
48. H.W. den Hartog, J.M. Rabenberg, and R. Pesch: *Met. Soc. B*., 1975, vol. 158, pp. 200–12.
49. H. Fredriksson and O. Nilsson: *Metall. Trans. B*, 1978, vol. 9B, pp. 111–20.
50. J. Campbell: *Castings*, 2nd ed., Butterworth, Amsterdam, 1991.
51. R. Mehrabian and M.C. Flemings: *Metall. Trans. B*, 1970, vol. 1B, pp. 455–64.
52. T. Fujii, D.R. Poirier, and M.C. Flemings: *Metall. Trans. B*, 1979, vol. 10B, pp. 331–39.
53. M. Wu, A. Ludwig, A. Bührig-Polaczek, M. Fehlbier, and P. Sahm: *Int. J. Heat Mass Transf*., 2003, vol. 46, pp. 2819–32.
54. P. Rouxa, B. Goyeau, D. Gobin, F. Fichot, and M. Quintard: *Int. J. Heat Mass Transf*., 2006, vol. 49, pp. 4496–4510.
55. M.C. Schneider and C. Beckermann: *Metall. Mater. Trans. A*, 1995, vol. 26A, pp. 2373–88.
56. J.P. Gu and C. Beckermann: *Metall. Mater. Trans. A*, 1999, vol. 30A, pp. 1357–66.
57. H. Combeau, M. Založnik, S. Hans, and P.E. Richy: *Metall. Mater. Trans. B*, 2009, vol. 40B, pp. 289–304.
58. M. Zaloznik and H. Combeau: *Int. J. Therm. Sci*., 2010, vol. 49, pp. 1500–09.
59. M. Wu and A. Ludwig: *Metall. Mater. Trans. A*, 2006, vol. 37A, pp. 1613–31.
60. M. Wu and A. Ludwig: *Metall. Mater. Trans. A*, 2007, vol. 38A, pp. 1465–75.
61. J. Li, M. Wu, A. Ludwig, and A. Kharicha: *Int. J. Heat Mass Transf*., 2014, vol. 72, pp. 668–79.
62. G. Lesoult: *Mater. Sci. Eng. A*, 2005, vols. 413–414, pp. 19–29.
63. K. Suzuki and T. Miyamoto: *Trans. Iron Steel Inst. Jpn*., 1978, vol. 18, pp. 80–89.
64. K. Suzuki and T. Miyamoto: *Trans. Iron Steel Inst. Jpn*., 1980, vol. 20, pp. 375–83.
65. J.J. Moore and N.A. Shah: *Int. Met. Rev*., 1983, vol. 28, pp. 338–56.
66. A. Ludwig, A. Kharicha, and M. Wu: *Metall. Mater. Trans. B*, 2014, vol. 45B, pp. 36–43.